WELDING RESEARCH

SUPPLEMENT TO THE *WELDING JOURNAL*, MAY 1988

Sponsored by the American Welding Society and the Welding Research Council

The Effect of Cooling Rate on Ferrite in Type 308 Stainless Steel Weld Metal

Ferrite content and composition show a significant dependence on cooling rate

BY J. M. VITEK AND S. A. DAVID

ABSTRACT. Weld filler metals such as Type 308 stainless steel generally solidify as primary ferrite, and during cooling the ferrite transforms to austenite. This transformation is normally not carried out to completion, resulting in some residual ferrite retained in the final as-welded microstructure. The effect of cooling rate on residual ferrite content and composition was evaluated by heating as-welded material to 1300°C (2372°F) and then cooling to room temperature at fixed rates that varied from 0.16° to 693°C/s (0.29° to 1247°F/s). As the cooling rate increased, the amount of retained ferrite increased, the ferrite's chromium content decreased, and its nickel content increased. The influence of the width of the elongated ferrite grains on the cooling rate effect was determined by examining ferrite regions of different sizes. Calculations using a simple diffusion model reproduced the experimental results qualitatively. The diffusion calculations provided additional information on the sensitivity of ferrite composition to cooling rate and ferrite width. The results of the present investigation can be combined with modelling results on cooling rates of welds to allow one to predict the amount and composition of ferrite in welds. Such information is necessary to understand the stability of ferrite under multiple-pass welding conditions or during elevated-temperature applications.

J. M. VITEK and S. A. DAVID are members of the Metals and Ceramics Division, Oak Ridge National Laboratory, Oak Ridge, Tenn.

Introduction

Austenitic stainless steels such as Type 308 are commonly used as weld filler metals. In order to reduce hot-cracking tendencies, alloy compositions are often chosen so that ferrite is the primary solidification phase (Refs. 1-9). Such a condition is achieved by allowing the ratio of the chromium to nickel equivalents (Cr_{Eq}/Ni_{Eq}) to be >1.35 (Ref. 10), as is the case for Type 308 stainless steel ($Cr_{Eq}/Ni_{Eq} \approx 1.6$). With ferrite as the primary solidification phase, segregation of tramp elements to the interdendritic areas is reduced because the solubility limits of these elements are generally greater in ferrite. Furthermore, during cooling, a solid-state transformation of ferrite to austenite occurs, and this insures that the solidification boundaries do not necessarily coincide with the grain boundaries in the final transformed structure, thereby reducing the susceptibility to cracking (Ref. 11).

During the cooling of welded structures, the transformation of ferrite to austenite does not proceed to completion and some residual ferrite is retained at room temperature. For example, 5 to 10% ferrite is typically found in Type 308 stainless steel welds. Based on a psuedobinary section of the Cr-Fe-Ni phase diagram, shown in Fig. 1, the ferrite composition in equilibrium with austenite at elevated temperatures and in metastable equilibrium with austenite at lower temperatures (Ref. 12) is expected to vary as a function of temperature. Results of isothermal aging studies (Ref. 12) have

KEY WORDS

Type 308 Stainless
Cooling Rate Effect
Ferrite Content
Ferrite Numbers
FN Numbers
1.6 Cr/Ni Equivalent
Ferrite Composition
Ferrite Distribution
Ferrite Stability
Diffusion Calculation

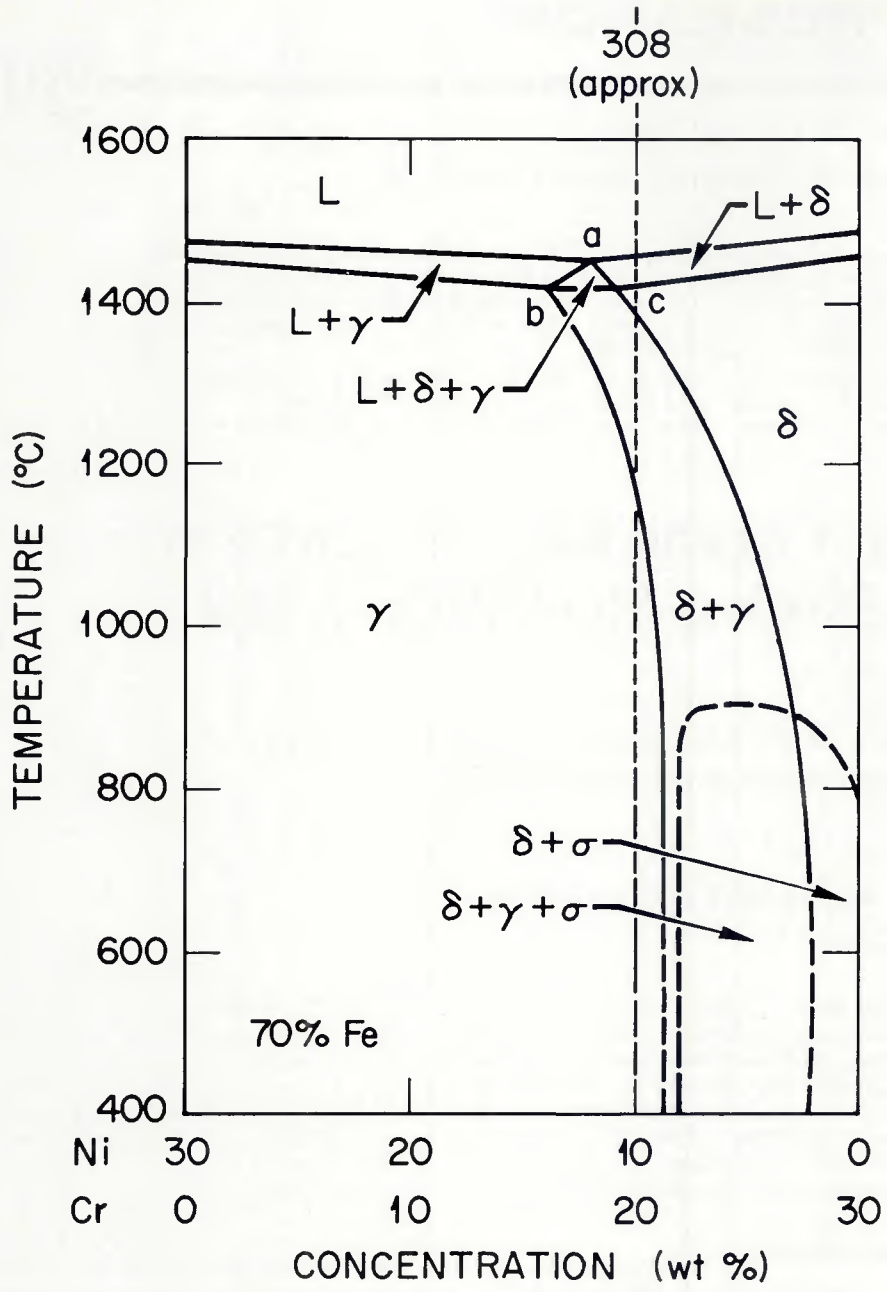

Fig. 1—Vertical section of the Fe-Ni-Cr ternary phase diagram, from Ref. 3

shown that the ferrite becomes richer in chromium and leaner in nickel as the temperature is decreased.

The cooling rate from elevated temperatures is expected to have an influence on the ferrite composition. During cooling, it can be assumed that the ferrite composition changes in order to maintain equilibrium (stable or metastable) until the diffusion kinetics are sufficiently slow to inhibit any further compositional changes. Such behavior has been described in detail elsewhere by introducing the idea of an effective quench temperature (Ref. 13). The objective of this paper was to quantitatively evaluate the dependence of ferrite composition on cooling rate. With such information, the ferrite composition can be predicted for various welding conditions. Knowing the ferrite composition would, in turn, be useful in understanding and predicting the stability of ferrite-containing weld microstructures during postweld exposures to elevated temperatures.

Experimental Procedures

In order to study the effect of cooling rate on ferrite composition, there are several desirable characteristics for the ferrite distribution. First, the width of the ferrite grains within the austenite matrix should be as uniform as possible since comparable diffusion distances are necessary when studying any cooling rate effects. Secondly, in order to be able to relate the results of this investigation to welding conditions, the ferrite must be relatively fine, comparable in size to the ferrite found in welds. Therefore, during specimen preparation, coarsening of the ferrite at elevated temperatures must be avoided. Finally, it is desirable to work with material containing a significant amount of ferrite (>5%) so that several ferrite areas can be readily located when doing transmission electron microscopy (TEM).

Table 1—Representative Composition of Type 308 Stainless Steel GTA Weld (wt-%)

Element	wt-%
Cr	20.18
Ni	9.35
Mn	1.74
Si	0.46
C	0.037
S	0.008
V	0.05
Ti	<0.01
Cu	0.09
B	0.002
P	0.016
Mo	0.09
Nb	<0.01
Co	0.06
Al	<0.01
N_2	0.060
Fe	Balance

To satisfy the above conditions as much as possible, it was decided to use as-welded Type 308 stainless steel, which contains ~10% ferrite. Although the ferrite grains are not perfectly uniform in width within the weld, as shown later in the results, the scale of the ferrite is reasonably constant throughout the weld. The examined material was restricted to the last pass of a multipass gas tungsten arc (GTA) weld in order to avoid any possible alterations that may arise during reheating of earlier passes. It should be noted, however, that the retained ferrite was in a metastable condition below approximately 1200°C (2192°F)—Fig. 1. The composition of a representative Type 308 stainless steel weld is given in Table 1.

Transverse slices, approximately 1 mm (0.04 in.) thick, were taken from a GTA weld and used for heat treating, ferrite number measurements, and eventual microstructural analysis. The heat treatment used to study the effect of cooling rate consisted of heating to 1300°C (2372°F), holding for a specified time, and then cooling at a fixed rate. The hold time at 1300°C was minimal in order to prevent any appreciable coarsening prior to cooling. Hold times were typically 30 s, although some samples were held for 3 and 5 min to check on the effect of hold

time. Based on earlier work (Refs. 12, 13), it was concluded that 30 s at 1300°C was sufficient time to bring the ferrite into equilibrium with the austenite. Most specimens were heat treated in a Gleeble thermomechanical simulator, in which a programmable constant cooling rate could be achieved. Some higher cooling rates could be achieved by carrying out an uncontrolled "free cool." The very highest cooling rates (>300°C/s—540°F/s) were achieved in a special furnace with forced gas cooling using thinner sheet specimens. Average cooling rates were calculated over the temperature range of 1300° to 800°C (2372° to 1472°F) and these values will be used when cooling rates are reported. Earlier work (Ref. 13) indicated this would be the temperature range of significance for these experiments. The cooling rates covered over three orders of magnitude, from a minimum of 0.16°C/s to a maximum of 693°C/s (0.29° to 1247°F/s).

The ferrite content, measured in terms of a ferrite number, was monitored before and after heat treating. Ferrite numbers were measured magnetically according to Ref. 14. A thin cross-sectional slice was cut from each welded and heat-treated section of material. TEM disks were machine-cut from the last pass section of the welds and were electropolished to produce thin-foil specimens. The microscopy was performed on a JEOL electron microscope at 200 keV. Ferrite compositions were measured by analytical electron microscopy (AEM). The probe sizes were on the order of 0.02 to 0.05 μm in diameter. The size was sufficiently small to insure that all analyses were made within the ferrite, without any contribution from neighboring austenite areas. X-ray spectra were recorded with a Tracor-Northern energy dispersive spectrometer. Hole counts were negligibly small and were ignored. Compositions were determined from the spectra for four elements, Fe, Cr, Ni and Mn, with the compositions normalized to 100%.

Fig. 2—Typical ferrite microstructure in austenite matrix

Several ferrite grains were examined for each condition, and several measurements were made within each ferrite grain, with the average values reported. Measurements were made within the central third of each ferrite grain to avoid any compositional gradients near the interfaces of the ferrite. Therefore, the measurements represent the bulk ferrite composition. In addition, the width of each ferrite region was determined. In separate work on homogenized Type 308 stainless steel, it was found the austenite composition did not vary with foil thickness. Therefore, compositions were measured in reasonably thick areas so that if any surface films were present on the electropolished foils, their influence would be insignificant.

Experimental Results

The ferrite distribution in the Type 308 welds consisted of elongated ferrite grains located at the dendritic cores, as described in detail by others (Refs. 15-20). A representative micrograph of ferrite in austenite is given in Fig. 2. The width of the ferrite regions was in the range of 0.5 to 4 μm. The amount of ferrite was evaluated and the results are presented in Table 2. The change in ferrite number as a function of cooling rate is shown in Fig. 3. There is a fair amount of scatter in the data, but this is common in welded materials (Ref. 20). In two cases, quite low values of ferrite number were detected before heat treating (2.2, 2.95). Because the measurements were on relatively thin specimens, it is possible the ferrite number depended on the sample thickness, and therefore, the absolute values for the ferrite numbers may not be very accurate. Consequently, the relative change in ferrite number was used to reduce the dependence of the results on specimen thickness and yield more reliable results. Such relative changes in ferrite number are also given in Table 2 and plotted in Fig. 3. A distinct relationship between cooling rate and relative change in ferrite content is found in Fig. 3. After cooling from 1300°C at the lowest rate, the ferrite level is quite low, well below the initial values. However, as the cooling rate from 1300°C is increased, the overall ferrite content also increases. At the highest cooling rates, substantially more ferrite is found than in the starting condition, indicating the cooling rate is much higher than in the GTA weld. It is also noteworthy that the holding time at 1300°C did not have any consistent influence on the ferrite levels.

Composition measurements revealed the presence of composition gradients within the ferrite, as shown in Fig. 4, which is a composition scan across a ferrite grain. However, it is clear from this

Table 2—Ferrite Numbers of Heat-Treated and Cooled Specimens

Cooling Rate ($\dot{T}$) (°C/s)	Hold Time At 1300°C (s)	Ferrite Number		
		Before	After	Relative change (%)
0.16	30	7.0	0.3	−96
0.16	180	6.2[a]	0.2	−97
0.98	30	5.0	1.9	−62
0.99	180	6.2[a]	1.6	−74
9.5	30	6.0	3.2	−47
10.1	180	6.2[a]	4.4	−29
79.0	180	6.2[a]	7.2	+16
93.0	30	2.95	4.2	+42
93.0	300	5.2	7.4	+42
103.0	30	4.2	4.7	+12
139.0	300	6.6	9.8	+48
275.0	30	2.2	4.2	+91

(a) Average value for several specimens; individual readings not taken before heat treating.

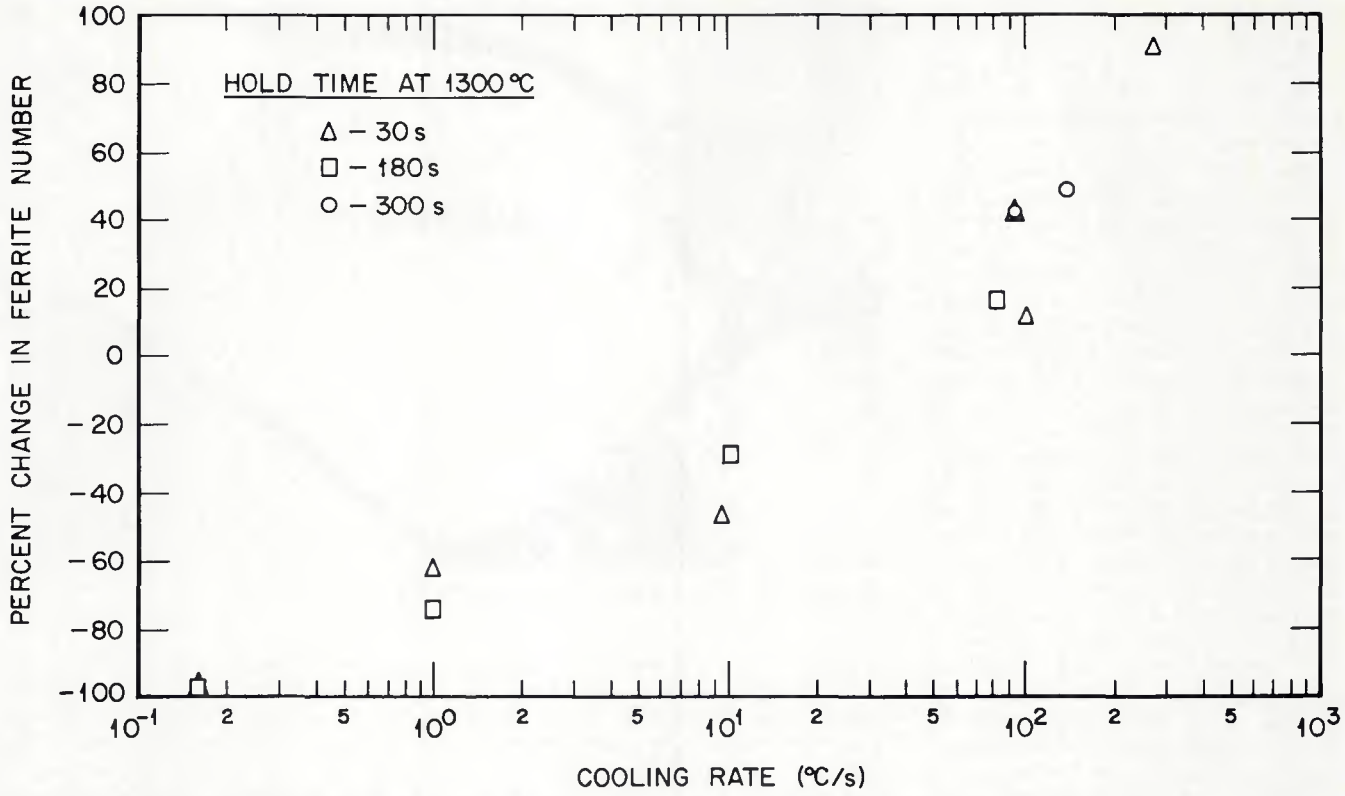

Fig. 3—Percent change in ferrite number as a function of the cooling rate from 1300°C. Hold times at 1300°C varied, as shown

figure that the ferrite composition was fairly uniform over approximately the central 60% of the ferrite, thereby assuring that the composition measurements made in the middle of the ferrite represented the bulk ferrite composition and were not affected by concentration gradients near the ferrite/austenite interface.

The ferrite composition was measured in the initial, as-welded condition. Several ferrite regions were evaluated, varying in width from 0.25 to 1.5 μm.[1] The average normalized ferrite composition (in wt-%) was 64.7Fe, 29.1Cr, 4.2Ni, 2.1Mn. Compared to the overall alloy composition given in Table 1, the ferrite is significantly enriched in chromium and depleted in nickel, with only a small enrichment in manganese. This agrees with the results from other studies (Refs. 12, 21).

The results of composition measurements of ferrite in samples cooled at different rates are given in Fig. 5. Only the results for chromium and nickel concentrations are presented. Manganese concentrations are not given because, as shown in Fig. 4, there was negligible partitioning of manganese between austenite and ferrite. Therefore, there was no significant effect of cooling rate on the manganese content of the ferrite. The iron concentrations are not presented because they are simply the complement of the chromium and nickel effects combined.

As noted in the procedure section, it is desirable to restrict the examination to ferrite grains of the same width. However, it was impossible to avoid some variation and range of ferrite sizes in the welds. Therefore, the data shown in Fig. 5 represent a restricted range of widths, and the data are grouped into three size classes. It is important to note that even if the ferrite grains were initially of uniform width, the dissolution of ferrite that occurs during cooling (Ref. 12) proceeds to different degrees, depending on the cooling rate (Ref. 13), and therefore the ferrite areas would not be uniform in width after cooling. The influence of ferrite size is treated in more detail in the following section.

Diffusion Model Calculations

Calculations were performed to aid in the understanding and interpretation of the experimental results. Although a very simple model was employed, the results are instructive. An iteration procedure was utilized. A constant cooling rate was approximated by step cooling in small increments. Equilibrium was assumed at the ferrite/austenite interface. The equilibrium composition as a function of temperature was taken from earlier results (Ref. 12). The internal ferrite composition was assumed to vary exponentially with time, based on the parameter-

$$\frac{Dt}{x^2}$$

where D is the temperature-dependent diffusion coefficient of chromium in ferrite, t is time, and x is the half-width of the ferrite. The composition of the ferrite was then calculated as a function of time for various cooling rates and ferrite widths. Several major assumptions are made. First, based on the relative values of diffusion coefficients, diffusion in austenite is considerably less than in ferrite and therefore was ignored. Second, dissolution of the ferrite was not taken into account although such dissolution has been observed (Ref. 12) and is necessary to account for the ferrite enrichment. Third, a simple exponential dependence of composition on time was assumed, but no account of the spatial dependence of composition was made. Finally, as the temperature decreased, only the interface composition and "bulk" composition were considered, without any regard to the composition profile within the ferrite. Nonetheless, the model can be instructive if the calculated concentrations are considered only qualitatively.

A representative plot of temperature, equilibrium concentration, and calculated composition vs. time for a specific ferrite width and cooling rate is shown in Fig. 6. As is clearly shown, the ferrite composi-

[1] *In general, the ferrite areas were narrower in the as-welded condition, indicating some coarsening took place upon heating to 1300°C.*

tion changes with decreasing temperature, trying to maintain equilibrium. However, beyond some point, the diffusion of chromium is too slow to keep up with the changing equilibrium concentration, and the ferrite composition changes very little with further cooling. This sequence has been described in detail elsewhere, and the temperature corresponding to the limiting chromium concentration has been identified as the effective quench temperature (Ref. 13). The influence of cooling rate is demonstrated in Fig. 6 by including the curves for two different cooling rates and keeping the ferrite width constant. With the present diffusion model, the effect of ferrite size can also be evaluated quite simply. A plot of the limiting chromium concentration vs. cooling rate for several ferrite half-widths is presented in Fig. 7. Since the equilibrium chromium concentration increases with decreasing temperature (Ref. 12), an increasing limiting value of the chromium concentration corresponds to a decreasing effective quench temperature. Qualitatively, the results of the simple diffusion calculations reveal the same general trends as those found experimentally in Fig. 5.

Discussion

The experimental procedure in this study was based on the assumption that two-phase equilibrium between ferrite and austenite was attained after a holding time of 30 s at 1300°C.[2] The results confirm the validity of this assumption. In Fig. 3, no consistent difference exists between the amount of ferrite present in samples held for 30 s, 3 min, or 5 min at 1300°C before cooling at a given rate. This indicates that equilibrium was reached within 30 s at 1300°C, with further exposure having no significant influence on the amount of ferrite present after cooling. Any deviations among samples cooled at the same rate, but held for different times, are assumed to be due to experimental uncertainty since the deviations are not uniform. The same conclusions can be drawn with regard to the effect of holding time after examining the data on ferrite composition in Fig. 5. These conclusions conform to expectations based on evaluation of the effective quench temperatures in these materials (Ref. 13). These earlier results showed that during the cooling of GTA welds, at cooling rates within the range examined in the present study, the elevated temperature microstructures basically maintain equilibrium until approximately 1000°C (1832°F). Therefore, it can be expected, and was confirmed by the present results, that equilibrium at 1300°C is achieved very quickly.

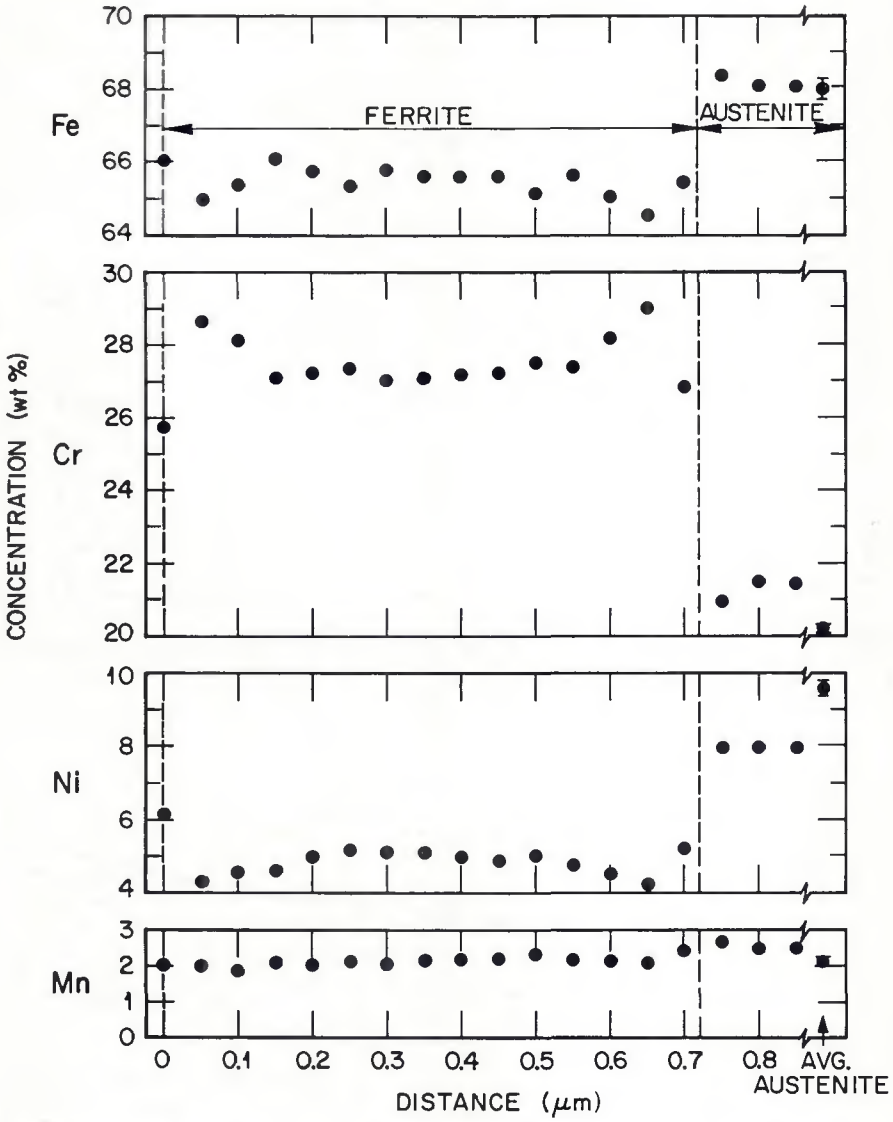

Fig. 4 — Concentration profile across a ferrite grain in a sample cooled from 1300°C at 25°C/s

The results show that the cooling rate has a significant impact on the amount of residual ferrite present in duplex austenite plus ferrite microstructures, as well as on the composition of the ferrite. Higher cooling rates retain greater amounts of ferrite and more effectively quench-in the ferrite composition in two-phase equilibrium at higher temperatures. The present results quantify these relationships. The data presented can be checked for internal consistency. Examination of Fig. 3 indicates that the amount of ferrite in the as-welded material did not change after heating to 1300°C and cooling at approximately 40°C/s (72°F/s). This implies the as-welded material was initially cooled at this rate, since re-heat treating did not alter the microstructure. Using this cooling rate and taking into account the fact that the ferrite is relatively fine, with a width on the order of approximately 0.5 μm, Fig. 5 indicates the as-welded ferrite should contain approximately 29% chromium and 4% nickel. This estimated composition is in good agreement with the measured composition of 29.1% Cr and 4.2% Ni, indicating the results on ferrite number and ferrite composition are consistent.

The experimental results shown in Fig. 5 indicate that at low cooling rates (0.1° to 10°C/s, or −0.18° to 18°F/s), the influence of the width of the ferrite areas is minimal. However, at high cooling rates (100° to 1000°C/s, or 180° to 1800°F/s), the ferrite width plays an important role. The results of calculations shown in Fig. 7 reveal a more uniform effect of ferrite size over the entire range of cooling rates considered. This discrepancy implies the model for calculating the ferrite composition at low cooling rates is not correct, and may be due to oversimplifying assumptions. For example, it may be

[2] *The nonequilibrium nature of coarsening of the ferrite is not considered here.*

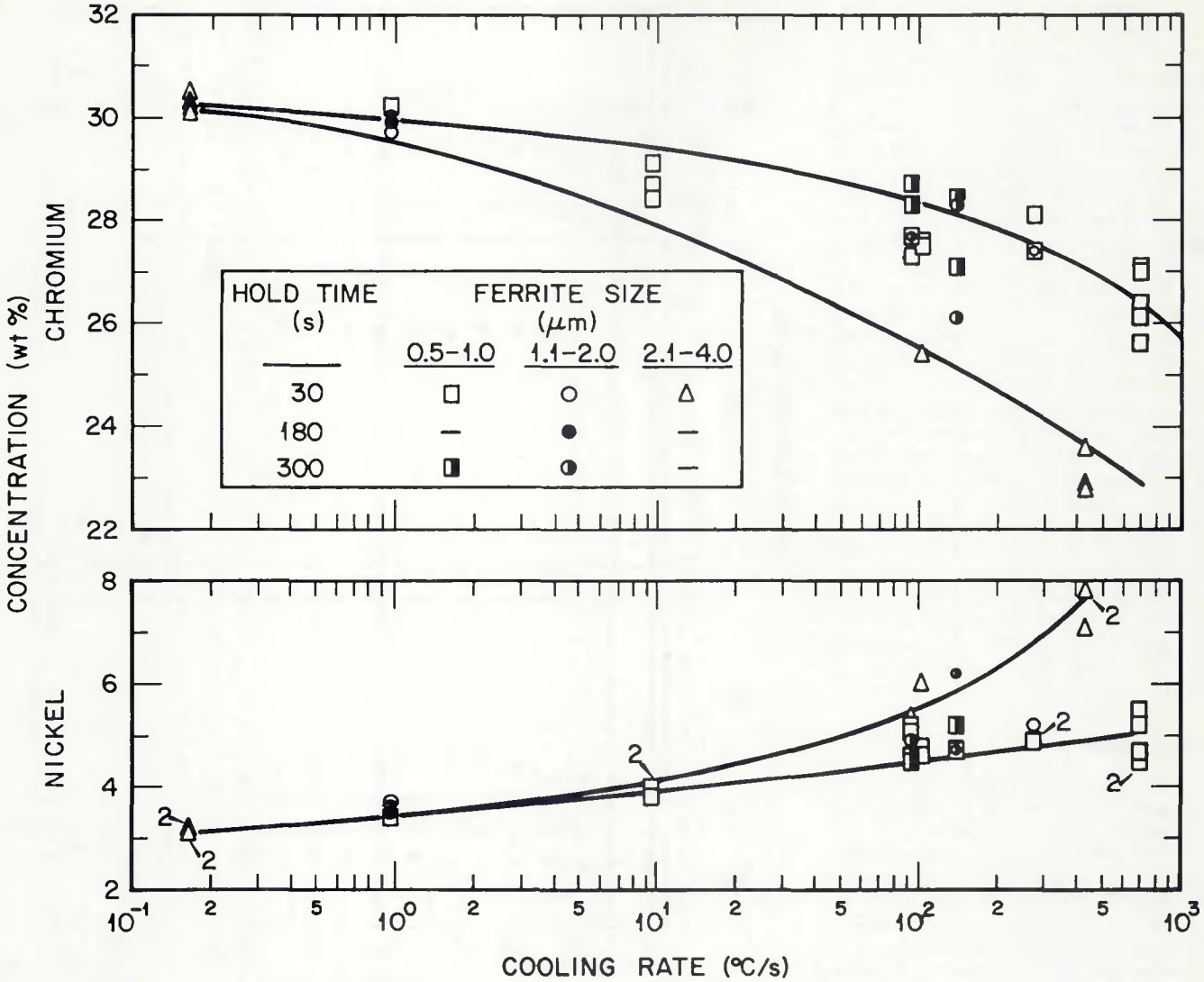

Fig. 5—Average ferrite composition vs. cooling rate. Data are divided according to ferrite size, as shown

inappropriate to ignore the dissolution of ferrite. Such dissolution is greatest at the lowest cooling rates, corresponding to the greatest amount of chromium enrichment. However, other factors may also play a role. The extrapolation of a linear relation between ferrite composition and temperature to the low temperatures, where diffusion still occurs at the lowest cooling rates, may not be valid. It is also possible that at the lower cooling rates chromium diffusion is no longer a rate-limiting step, thus invalidating the theoretical calculations. Finally, at the lower cooling rates, diffusion within the austenite may occur, and this was ignored in the model. Whatever the cause, the experimental results show less influence of ferrite width at low cooling rates.

At higher cooling rates, the effect of ferrite width is significant. In an earlier study (Ref. 13), the effective quench temperatures of GTA and laser beam welds were found to be comparable. Without considering the effect of ferrite width, it was concluded that the solid state cooling rates were comparable in the two techniques. However, the present results indicate that under the relatively high cooling rate conditions for laser beam welding, ferrite width cannot be ignored. The data in Fig. 7 for equivalent final chromium concentrations (*i.e.*, equivalent effective quench temperatures) can be used to show that the cooling rate ($\dot{T}$) and ferrite width (W) are approximately related by $\dot{T} \propto \frac{1}{W^2}$. Thus, for the case of laser beam welds, with ferrite areas approximately 1/10 the size of the ferrite regions in GTA welds, these results indicate the solid-state cooling rate for laser beam welds was approximately 100 times as great as the cooling rate of the GTA welds. Such a conclusion seems to be quite reasonable.

In addition to the diminished influence of ferrite width on the ferrite composition at low cooling rates, the curves in Fig. 5 also level off at lower cooling rates. This means the effect of cooling rate on ferrite composition is reduced at lower cooling rates. Therefore, for processes such as submerged arc and electroslag welding, where the cooling rates are relatively low, the effect of changing cooling rate will be small. With regard to ferrite content (rather than ferrite composition), Fig. 3 shows ferrite content decreases with decreasing cooling rate, although the sensitivity is not as great as at higher cooling rates. Experimental observations of materials solidified and subsequently cooled in the low-cooling rate range have shown essentially no change in ferrite content with varying cooling rate (Refs. 20, 22). This apparent discrepancy can be reconciled by realizing that in the present study, the starting condition, and in particular the scale of the ferrite, was identical before cooling at different rates. In the earlier work, different solidification rates, as well as different solid-state cooling rates, were employed. Thus, at lower solidification rates, significantly coarser

structures were produced, and apparently the size differences were large enough to compensate for the tendency to retain less ferrite at the lower cooling rates.

On the other hand, ferrite content should be quite sensitive to cooling rate in the range of high cooling rates. The results of the present study show ferrite content increases and ferrite chromium concentration decreases with increasing cooling rate. Recent work (Ref. 23) on a variety of laser beam welded austenitic stainless steels has revealed this predicted behavior exactly. By varying the laser power, different cooling rates were achieved, and ferrite numbers varied by up to 100%. If, however, solidification rates are extremely high and beyond some critical level, the mode of solidification may change from primary ferrite to primary austenite and the effect of cooling rate on the ferrite content and composition that is described in this paper is inapplicable. With a change in the solidification mode to primary austenite formation, there is essentially no ferrite present at elevated temperatures to transform to austenite, and so the influence of cooling rate on the extent of this transformation is meaningless. Such high solidification rates have been achieved with splat quenching and under some laser beam welding conditions, leading to a change in the solidification mode and producing essentially ferrite-free microstructures (Refs. 23, 24).

The influence of cooling rate on both the ferrite content and its composition

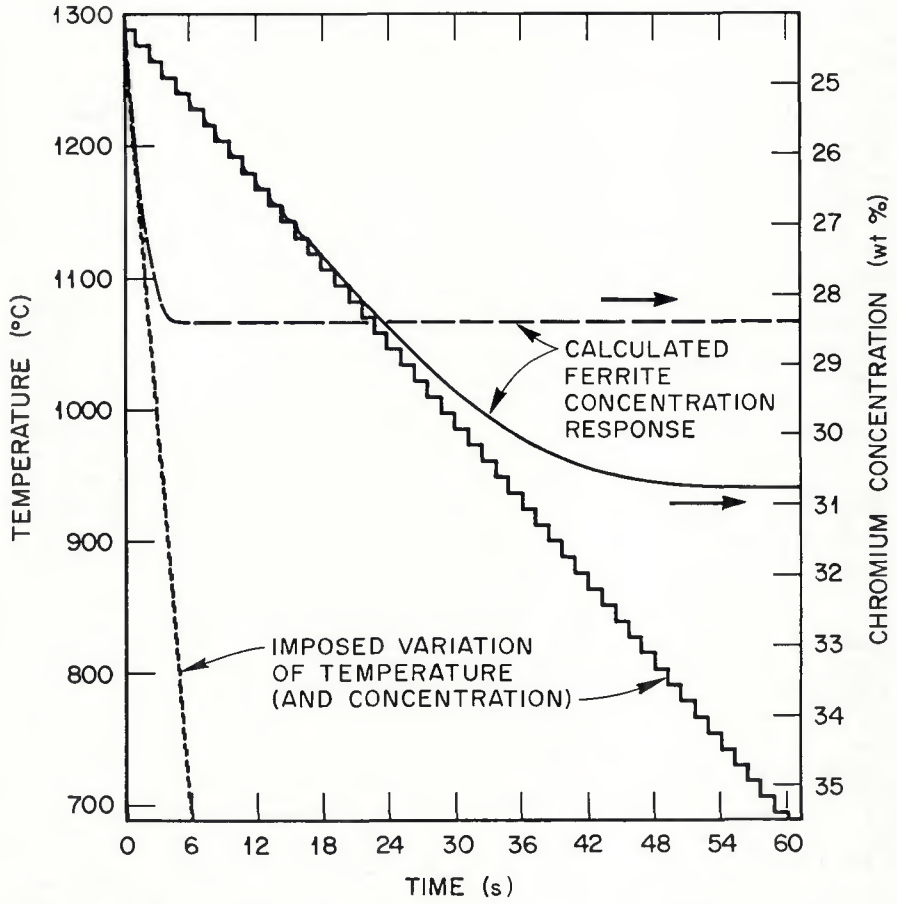

Fig. 6 — Plot of stepwise-approximated variation in temperature and equilibrium chromium concentration vs. time during cooling, and calculated continuous change in bulk ferrite composition vs. time. Calculations are for ferrite of 0.5 μm half-width, cooled at 10°C/s (solid lines) and 100°C/s (broken lines)

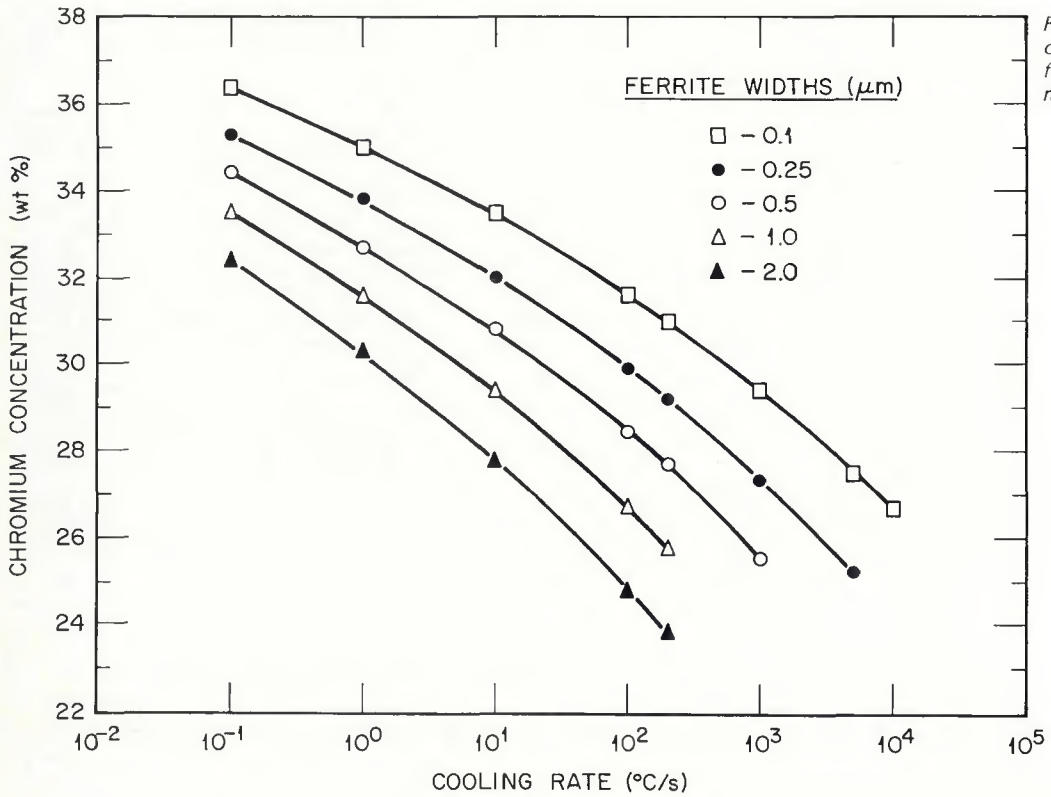

Fig. 7 — Calculated limiting chromium concentration in ferrite as a function of cooling rate and ferrite size (half-width)

has been determined quantitatively in this study for Type 308 stainless steel. This information can be used to evaluate the numerous models which have been utilized to predict thermal histories in the fusion zones (FZ) and heat-affected zones (HAZ). By evaluating the ferrite composition at various locations, the accuracy of the model predictions can be verified. Once such model verification has been performed, the modelling studies can be used with reliability to determine the cooling rates throughout the weld and HAZ. The present study can then be employed to relate these calculated cooling rates to the amount of ferrite present in the weld and its composition. Eventually, the combination of the present results on cooling rate effects and the modelling studies can be used to predict the effect of varying welding conditions on the microstructure. In order to make this prediction capability complete, the scale of the ferrite structure must be shown as a function of solidification conditions. Such a predictive capability is desirable since knowledge of the ferrite content and its composition is necessary in trying to understand the stability of ferrite-containing weld microstructures.

Conclusions

The ferrite content and ferrite composition of duplex Type 308 austenitic stainless steel welds were evaluated as a function of cooling rate over the range of 0.16 to 693°C/s (0.29° to 1247°F/s). It was found that as the cooling rate increased, the amount of residual ferrite at room temperature also increased, while the chromium concentration decreased and the nickel content increased. The results agree with a previously proposed model in which ferrite maintains metastable equilibrium with austenite while cooling down to an effective quench temperature, which is cooling-rate dependent. Diffusion calculations supported the experimental results and the measured dependence of composition on cooling rate. The results also indicate that ferrite achieves equilibrium with austenite within a few minutes when heated to 1300°C (2372°F). Earlier studies have shown the same general trends for the ferrite composition dependence on cooling rate. However, with the quantitative relationships obtained in this study, it may be possible to use this information to verify modelling calculations. Eventually this information may be used to predict weld microstructures. Such information is vital in understanding ferrite stability when welds are exposed to elevated temperatures, either as a result of multipass welding or during service.

Acknowledgments

The authors would like to acknowledge the technical assistance of R. W. Reed in the preparation and evaluation of specimens. The authors also wish to acknowledge the efforts of R. L. Klueh and D. N. Braski in reviewing the manuscript, and the work of Kathy Gardner in the preparation of the manuscript. The research was sponsored by the Division of Materials Sciences, U.S. Department of Energy, under contract DE-AC05-840R21400 with the Martin Marietta Energy Systems, Inc.

References

1. Borland, J. C., and Younger, R. N. 1960. Some aspects of cracking in austenitic steels. *British Weld. J.* 7(1):22-60.

2. Hull, F. C. 1967. Effect of delta ferrite on the hot cracking of stainless steel. *Welding Journal* 46(9):399-s to 409-s.

3. Masumoto, I., Tamaki, K., and Kutsuna, M. 1972. Hot cracking of austenitic stainless steel weld metal. *Journal of JWS* 41(11):1306-1314, Brutcher Transl. 8965/1973.

4. Thier, H. 1975. Schweissen hochlegierten Stahle. *DVS-Berichte,* 33:69-75.

5. Arata, Y., Matsuda, F., and Katayama, S. 1976. Solidification crack susceptibility in weld metals of fully austenitic stainless steel (report 1) — fundamental investigation of solidification behavior of fully austenitic and duplex microstructures and effect of ferrite on microsegregation. *Trans. of the Japanese Welding Research Institute* 5(2):35-51.

6. Brooks, J. A., and Lambert, F. J., Jr. 1978. The effect of phosphorus, sulfur, and ferrite content on weld cracking of Type 309 stainless steel. *Welding Journal* 57(5):139-s to 143-s.

7. Kujanpää, V., Suutala, N., Takalo, T., and Moisio, T. 1979. Correlation between solidification cracking and microstructure in austenitic-ferritic stainless steel welds. *Weld. Res. Inter.* 9(2):55-76.

8. Lippold, J. C., and Savage, W. F. 1982. Solidification of austenitic stainless steel weldments: part III — the effect of solidification behavior on hot cracking susceptibility. *Welding Journal* 61(12):388-s to 396-s.

9. Brooks, J. A., Thompson, A. W., and Williams, J. C. 1984. A fundamental study of the beneficial effects of delta ferrite in reducing weld cracking. *Welding Journal* 63(3):71-s to 83-s.

10. MacIsaac, D. G., Shiohara, Y., Chu, M. G., and Flemings, M. C. *Grain Refinement in Castings and Welds.* Ed. G. J. Abbaschian and S. A. David, TMS-AIME, Warrendale, Pa., pp. 87-95.

11. Kujanpää, V. P., David, S. A., and White, C. L. 1986. Formation of hot cracks in austenitic stainless steel welds — solidification cracking. *Welding Journal* 65(8):203-s to 212-s.

12. Vitek, J. M., and David, S. A. 1985. Metastable equilibrium of ferrite in Type 308 stainless steel. *Scripta Metall.* 19:23-26.

13. Vitek, J. M., and David, S. A. 1985. The concept of an effective quench temperature and its use in studying elevated-temperature microstructures. *Metall. Trans.* 16A:1521-1523.

14. AWS A4.2-74, *Standard Procedures for Calibrating Magnetic Instruments to Measure the Delta Ferrite Content of Austenitic Stainless Steel Weld Metal.* American Welding Society, Miami, Fla.

15. Goodwin, G. M., Cole, N. C., and Slaughter, G. M. 1972. A study of ferrite morphology in austenitic stainless steel weld metals. *Welding Journal* 51(9):425-s to 429-s.

16. Takalo, T., and Moisio, T. 1976. Influence of ferrite content on its morphology in some austenitic weld metals. *Metall. Trans.* 7A:1591-1592.

17. Lai, J. K., Nath, B., and Townsend, R. D. April 1979. Variations in delta-ferrite content and morphology in a multipass Type 316 weldment and their effect on creep rupture properties. British Nuclear Energy Society, *Conference on Welding and Fabrication in the Nuclear Industry,* London, England.

18. Suutala, N., Takalo, T., and Moisio, T. 1979. Relationship between solidification and microstructure in austenitic and austenitic-ferritic stainless steel welds. *Metall. Trans.* 10A:512-514.

19. Suutala, N., Takalo, T., and Moisio, T. 1979. Single phase ferritic solidification mode in austenitic-ferritic stainless steel welds. *Metall. Trans.* 10A:1183-1190.

20. David, S. A. 1981. Ferrite morphology and variations in ferrite content in austenitic stainless steel welds. *Welding Journal* 60(4): 63-s to 71-s.

21. David, S. A., Goodwin, G. M., and Braski, D. N. 1979. Solidification behavior of austenitic stainless steel filler metals. *Welding Journal* 58(11):330-s to 336-s.

22. Suutala, N. 1983. Effect of solidification conditions on the solidification mode in austenitic stainless steels. *Met. Trans.* 14A:191-197.

23. David, S. A., Vitek, J. M., and Hebble, T. L. 1987. Effect of rapid solidification on stainless steel weld metal microstructures and its implications on the Schaeffler diagram. *Welding Journal* 66(10):289-s to 300-s.

24. Vitek, J. M., DasGupta, A., and David, S. A. 1983. Microstructural modification of austenitic stainless steels by rapid solidification. *Metall. Trans.* 14A:1833-1841.